Thin Solid Films 541 (2013) 46–50

Contents lists available at SciVerse ScienceDirect

Thin Solid Films

journal homepage: www.elsevier.com/locate/tsf

Nondestructive mapping of chemical composition and structural qualities of group III-nitride nanowires using submicron beam synchrotron-based X-ray diffraction

P.L. Bonanno [a,*], S. Gautier [b], Y.El. Gmili [c], T. Moudakir [c], A.A. Sirenko [d], A. Kazimirov [e], Z.-H. Cai [f], J. Martin [b], W.H. Goh [a], A. Martinez [g], A. Ramdane [g], L. Le Gratiet [g], N. Maloufi [h], M.B. Assouar [i], A. Ougazzaden [a]

[a] Georgia Institute of Technology/GTL, UMI 2958 Georgia Tech-CNRS, 57070 Metz, France
[b] LMOPS + UMI: Laboratoire Matériaux Optiques, Photonique et micro-nano Systèmes, UMR CNRS 7132, Université de Metz et SUPELEC, 2 rue E. Belin, 57070 Metz, France, UMI 2958 Georgia Tech-CNRS, 57070 Metz, France
[c] UMI 2958 Georgia Tech-CNRS, 57070 Metz, France
[d] Department of Physics, New Jersey Institute of Technology, Newark, NJ 07102, USA
[e] Cornell High Energy Synchrotron Source (CHESS), Cornell University, Ithaca, NY 14853, USA
[f] Advanced Photon Source, 9700 S. Cass Avenue, Argonne, IL 60439, USA
[g] Laboratoire de Photonique et de Nanostructures, UPR CNRS 20, Route de Nozay, 91460 Marcoussis, France
[h] Laboratoire d'Etude des Textures et Application aux Matériaux UMR CNRS 7078 Ile du Saulcy 57045 METZ cedex 1, France
[i] Laboratoire de Physique des Milieux Ionisés et Applications, Nancy University, CNRS, BP 239, F-54506 Vandoeuvre-lès-Nancy Cédex, France

ARTICLE INFO

Available online 7 January 2013

Keywords:
Nondestructive
GaN
Synchrotron
X-ray diffraction
Nano
Nanowire
RSM
MQW

ABSTRACT

Submicron beam synchrotron-based X-ray diffraction (XRD) techniques have been developed and used to accurately and nondestructively map chemical composition and material quality of selectively grown group III-nitride nanowires. GaN, AlGaN, and InGaN multi-quantum-well nanowires have been selectively grown on lattice matched and mismatched substrates, and the challenges associated with obtaining and interpreting submicron beam XRD results are addressed and solved. Nanoscale cathodoluminescence is used to examine exciton behavior, and energy-dispersive X-ray spectroscopy is used to verify chemical composition. Scanning transmission electron microscopy is later used to paint a more complete picture. The advantages of submicron beam XRD over other techniques are discussed in the context of this challenging material system.

1. Introduction

Nanoheteroepitaxy is a promising approach for integration of dissimilar materials that have complementary electrical and optical properties [1–3]. This technique is especially important for GaN and other group III-nitride based structures that in the thin-film form tend to suffer from high density of treading dislocations due to the large lattice and thermal mismatch with conventional substrates, such as sapphire and SiC.

At the same time, enhanced confinement and temperature stability of the threshold current have attracted attention to 1- and 2-dimensional group III-nitride structures for use in high-speed nano high electron mobility transistors, high density data storage devices, blue light-emitting diodes, nanofluidic biochemical sensors, and quantum dot lasers [4]. Also, quantum well structures grown on semi-polar planes have shown reduced piezolectric effects that could otherwise reduce the luminescence efficiency [5,6].

Progress in this emerging field of nanotechnology depends heavily on utilization of advanced material characterization tools, such as synchrotron radiation high resolution sub-micron beam X-ray diffraction (XRD) [7–10], which has been recently applied to various material systems and device structures, demonstrating the capability to measure strain relaxation at the sidewalls of micron-wide waveguide ridges [7] and to reveal details of inter- and intrafacet surface migration [8]. Currently, there is substantial interest in knowing the variation of structural properties on the nano scale that is being satisfied by combining nondestructive techniques such as high-resolution XRD and reciprocal space mapping, with real-space mapping on the nanoscale [8,9]. In this paper, problems related to using X-ray diffraction on nanoscale group III nitrides grown by nano selective area growth (NSAG) are addressed, and results are presented for InGaN/GaN multi-quantum-well (MQW) nanoridges, AlGaN/GaN nanoridges, and overgrown GaN-on-AlN nanoridges.

* Corresponding author.
E-mail address: plb2@njit.edu (P.L. Bonanno).

0040-6090/$ – see front matter © 2013 Elsevier B.V. All rights reserved.
http://dx.doi.org/10.1016/j.tsf.2012.12.099

2. Experimental details

2.1. Apparatus and measurements

Submicron beam X-ray diffraction was performed using 10.4 keV synchrotron-based light at the 2-ID-D beamline of the Advanced Photon Source at Argonne National Labs. Our complete setup is shown in Fig. 1. A zone-plate focused the ~100 mA beam to a spot size of around 240 nm. An order sorting aperture blocked higher order foci from reaching the sample. The focusing of the X-ray radiation resulted in a photon momentum spread of around 180 arc sec, which limited our angular resolution in the ω and χ angles. We opted to measure around the (0 0 . 4) and (1 0 . 5) reflections of our samples because these regions of reciprocal space provide good intensity and a high Bragg angle θ_B, which serves to minimize the footprint of the beam on the sample surface, which varies as $1/\sin\theta_B$.

To collect diffracted photons, we used either a single channel detector equipped with a slit or a CCD detector, switching between them depending on the needs of each particular measurement. The CCD detector's inter-pixel distance corresponded to about 8 arc sec. This, combined with our photon momentum spread, resulted in a strain accuracy of ±0.0003 at our chosen reflection orders. Detectors were mounted on the 2θ arm of a goniometer. An XYZ sample stage that provided lateral sample positioning with 50 nm precision was mounted near the center of the goniometer.

During all experiments, a fluorescence detector was used to measure Ga-*K*, In-*L*, and Fe-*K* fluorescence to help us monitor our location on the sample.

Due to the small scale of our structures, special care was taken to align the sample surface directly with the axis of θ rotation. This step was crucial to our spatial resolution, as it prevented the beam from wandering the sample surface during rocking experiments. It is a step often overlooked in sub-micron beam XRD and is explained in more detail in Ref. [11].

Room-temperature CL measurements were carried out using a Zeiss Supra 55VP digital scanning electron microscope. Emission was gathered by a parabolic mirror collector to be analyzed by a Horiba JobinYvon iHR320 spectrometer, providing a spectral resolution of 0.06 nm. Samples were prepared for scanning transmission electron microscopy (STEM) and cross-sectional energy-dispersive X-ray spectroscopy (EDX) by using focused ion beam thinning and ion milling. In a clean room (ex situ), a 50 nm-thick layer of carbon, followed by a 100 nm layer of Si_3N_4, was applied to the sample surface from a platinum mask used to define the shape of the milling lamina. Then, using Ga^+ ions, the sample is cut to cross-sections around 100 nm thick. Previous experiments have shown that incidental implantation of gallium does not change the final composition by more than the precision of EDX. STEM images and EDX measurements were performed in an aberration-corrected JEOL 2200FS microscope operating at 200 kV with a probe current and probe full width at half maximum of 150 pA and 0.12 nm, respectively. Scanning electron microscopy (SEM) measurements were performed on a Zeiss Supra 55VP operating in secondary electron imaging mode with an accelerating voltage of 15 kV and a working distance of 10 mm.

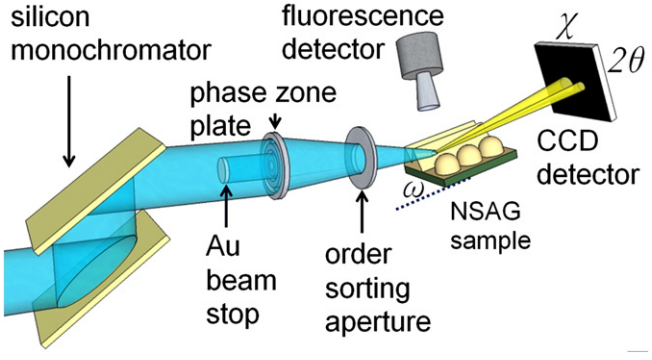

Fig. 1. Our setup at the 2-ID-D beamline of the Advanced Photon Source in Argonne National Labs. The semi-transparent blue represents the 10.4 keV beam.

2.2. Samples

Group III-nitride nanowires were grown by NSAG in a metal organic vapor phase epitaxy (MOVPE) T-shape reactor as follows [12]: first, chemical vapor deposition was used to deposit a 140 nm layer of SiO_2 on (0001)-oriented GaN-on-Al_2O_3 and AlN-on-Al_2O_3 templates. Reactive ion etching was then used to create 10×10 μm^2 dielectric masks in a field of bare template. Then, electron-beam lithography was used to pattern multiple nano-stripe-shaped windows through the mask. These windows are 120 nm wide and 7.6 μm long and are each oriented in one of two (<1–1 0 0> or <1 1–2 0>) crystallographic directions. The bare template exposed through these windows allowed them to act as nucleation sites for subsequent MOVPE growth of group III-nitride nanowires. This growth was carried out in ambient nitrogen, using trimethylindium, trimethylgallium, trimethylaluminum, and ammonia as sources of indium, gallium, aluminum, and nitrogen respectively. Low-growth-rate conditions at this stage help achieve high selectivity and crystalline quality.

Three NSAG samples were grown for this study. The first one is GaN, grown using an AlN-on-Al_2O_3 template. GaN was grown in 60 kPa of ambient nitrogen at 1000°. The second one is AlGaN grown on a GaN-on-Al_2O_3 template at 13.3 kPa and 1000°°C. The third sample is an InGaN/GaN MQW structure grown at 13.3 kPa and 1000 °C by switching on and off the presence of trimethylindium to create InGaN quantum wells that are a few nanometers thick.

All samples used were imprinted with a large grid of markers, either SiO_2 or Fe. these markers were around 4 μm wide and 1 mm long, making them easy to find by scanning for Fe-*K* fluorescence or drops in Ga-*L* or In-*L* fluorescence. The sample was mapped so that we know the locations of the 10×10 μm^2 dielectric masks relative to the marker grid pattern.

3. Calculations

Traditionally, X-ray diffraction signals are expected to be slightly offset and corrected for by using an angularly proximate reference signal such as the diffraction peaks from the substrate. However, in diffraction of material systems where the substrate signal is extremely far from the signal of interest, this method is not practical. Tiny misalignments in sample mounting cause the reciprocal space of the sample to rotate unpredictably relative to the goniometer. This can be accounted by using two reference signals to deduce the parameters of that rotation [11].

If diffracted signal is collected using a CCD detector, then misalignment between the detector and the goniometer needs to be accounted for before any data is taken, including reference signal data mentioned above. This misalignment has 6° of freedom and the method of correcting for it can be found in [11].

3D reciprocal space mapping was performed using CCD images taken at multiple values of ω. First, we use our deduced CCD parameters and misalignments (L,α,β,γ) to assign pixel positions (Δx_p,Δy_p) to angle space offsets from the goniometer position [11]

$$\Delta 2\theta = \arcsin\left(\frac{\Delta y_{2\theta}\cdot\cos\alpha}{\sqrt{L^2+\Delta y_{2\theta}^2+2L\Delta y_{2\theta}\cdot\sin\alpha}}\right)$$

$$\Delta\chi = \arcsin\left(\frac{\Delta x_{\chi}\cdot\cos\beta}{\sqrt{L^2+\Delta x_{\chi}^2+2L\Delta x_{\chi}\cdot\sin\beta}}\right),$$

where

$$\begin{pmatrix} \Delta x_\chi \\ \Delta y_{2\theta} \end{pmatrix} = \begin{pmatrix} \cos(-\gamma) & -\sin(-\gamma) \\ \sin(-\gamma) & \cos(-\gamma) \end{pmatrix} \begin{pmatrix} \Delta x_p \\ \Delta y_p \end{pmatrix}.$$

Once we have signal in 3D angular space (ω,2θ,χ), we can transform into reciprocal lattice space using conventional equations: $q_x = (2/\lambda) \cdot \sin(2\theta/2) \cdot \cos(\omega - 2\theta/2) \cdot \sin\chi$; $q_y = (2/\lambda) \cdot \sin(2\theta/2) \cdot \sin(\omega - 2\theta/2)$; $q_z = (2/\lambda) \cdot \sin(2\theta/2) \cdot \cos(\omega - 2\theta/2) \cdot \cos\chi$.

To then obtain chemical composition from this lattice information, we used the method put forth by Schuster et al. in Reference [13], using low-pressure elastic constants reported in Reference [14].

4. Results

4.1. InGaN/GaN MQW nanowires

An SEM image in Fig. 2a shows the layout of the sample, and a red circle indicates the region where measurements were performed to obtain results shown in Fig. 2b, c, e, and f. Fig. 2b shows a cross sectional STEM where the MQW structure is clearly shown, and Fig. 2c shows a zoomed-in portion of the MQW structure where indium-rich nanowires have formed. Indium incorporation values denoted on the image were obtained through destructive cross-sectional EDX.

Fig. 2e and f shows CL and XRD results respectively, both of which were obtained from the region denoted in Fig. 2a prior to sacrificing the sample. With proper choice of bowing parameter (1.4 eV), the CL results would roughly correspond to an indium incorporation of about 10%, corroborating our XRD and EDX results. In the general case, however, there are quantum effects due to the MQW structure which strongly influence exciton transitions. The XRD results lead one directly and certainly to the correct indium incorporation. Asymmetric XRD measurements (not shown) indicate completely pseudomorphic growth in the MQW structure, as expected for this system.

Fig. 2d shows a spatial $In_{0.06}Ga_{0.94}N$ diffraction scan over the span of the 10 μm mask. The spatial axis can be related directly to the SEM layout in Fig. 2a (which is why the two are positioned this way relative to each other). The field and individual nanoridges can be clearly discerned, and in fact the diffraction pattern is extremely uniform across the different ridges (differences in intensity can be shown to arise from beats due to sampling frequency.), indicating a very uniform crystallographic orientation of the different ridges.

4.2. AlGaN nanoridges

An SEM image in Fig. 3a shows the layout of the sample, with a red circle indicating the region where the 2D reciprocal space map in Fig. 3b was measured, and a blue circle indicating the region where the 3D reciprocal space map in Fig. 3d was measured. The latter includes lattice data from 3 distinct ridges.

Fig. 3c is a collection of (1 0 . 5) diffraction scans taken at regularly spaced positions across the 10 μm mask width. As with Fig. 2d, the lateral axis correlates quite accurately with the SEM layout above it (Fig. 3a), and it's clear which ridges are responsible for which signals (The strong red 'band' is due to the GaN template under the SiO_2 mask). The y axes have been converted from angle space into lattice parameter (left) and aluminum incorporation (right). "Missing" signals indicate a nonuniformity in lattice orientation across the different ridges.

4.3. GaN ridges on AlN template

Two GaN nanoridges were overgrown until they began to coalesce. The entire 2-ridge structure is about 1.5 μm wide and 9 μm long. Our beam was moved laterally across the two ridges at the Bragg conditions for (0 0 . 4) while our CCD detector collected diffraction signal images. Multiple secondary signals were noted, which moved in χ as we scan across the ridge structure. A summary of the

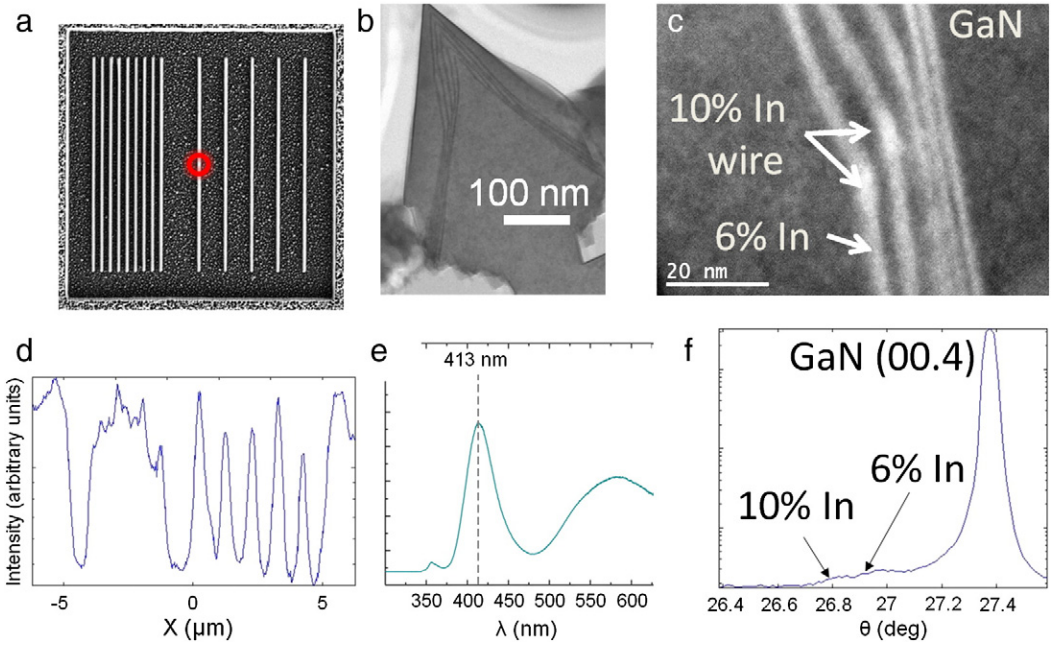

Fig. 2. a) SEM image taken of the 10×10 μm² mask region in the InGaN/GaN MQW nanowire sample, showing the layout of the nanoridges. The red circle indicates the "central ridge" where data was taken for b, c, e, and f. b) Bright field STEM image of the central ridge showing the MQW structure. c) Close up of a high angle annular dark field STEM image of the area shown in subpanel b with labels indicating EDX chemical analysis results, measuring indium concentrations. Two indium-rich nanowires are indicated by "10% In wire." d) Diffraction intensity taken by scanning across the 10 μm mask region in the direction perpendicular to the nanoridges at Bragg conditions optimized for $In_{0.06}Ga_{0.94}N$. The X axis corresponds exactly to the SEM image in subpanel a above. e) CL spectrum taken at the central ridge. f) XRD θ–2θ scan performed on the central ridge, clearly showing the two InGaN signals and the GaN signal.

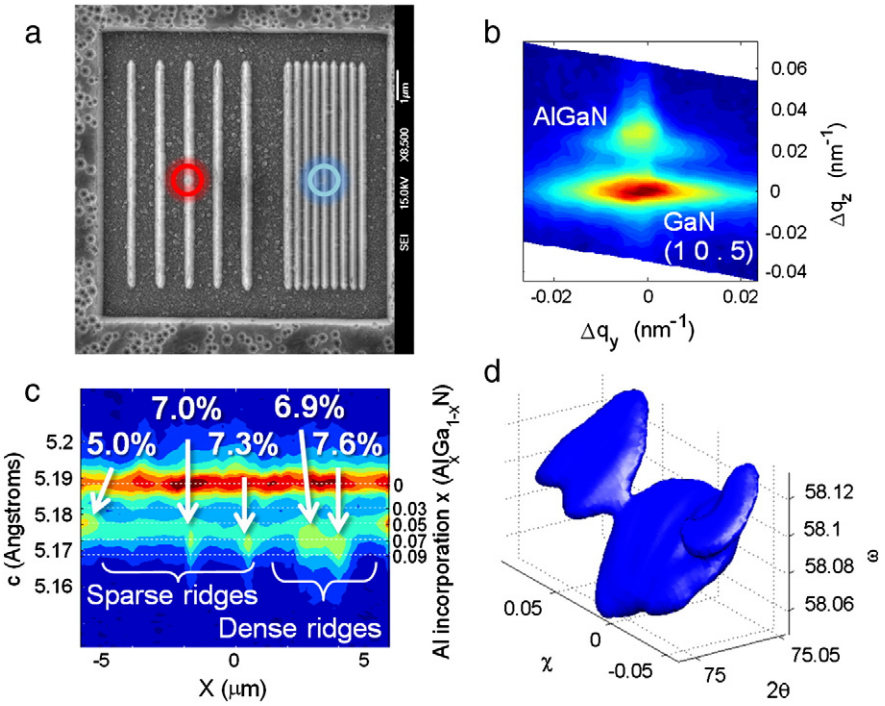

Fig. 3. a) SEM image taken of the 10×10 μm^2 mask region in the AlGaN nanoridge sample, showing the layout of the nanoridges. The red circle indicates the location where the data was taken for b and the blue circle indicates the location where the data was taken for d. b) 2D reciprocal space map of the (1 0 . 5) reflection, taken at the location denoted by the red circle in subpanel a. c) X-scan of diffracted intensity measured with a single channel detector for the (0 0 . 6) reflection across the center of the 10×10 μm^2 mask area in the direction perpendicular to the nanoridges. The Y axes are lattice parameter (left) and aluminum incorporation (right). Aluminum composition %s corresponding to some signals are noted. d) 3D reciprocal space map of 3 different ridges, represented by a 75% isointensity surface. The central signal is strongest because it originates from the ridge under the strongest central part of our X-ray beam, which was centered at the position denoted by the blue circle in subpanel a.

data is shown in Fig. 4a, along with a diagram of a planar configuration which would be responsible for such an effect.

Fig. 4b shows CL data taken at 18 different positions across the same 2-ridge structure. The spatial axis corresponds roughly with the diagram in Fig. 4a. The signal is GaN luminescence (~365 nm) and the intensity can be seen to vary with position. The signal is weakest at the crests of the ridges, where XRD results in Fig. 4a indicate planar discontinuity, and is strongest at the sidewalls. The signal then becomes weaker as the ridge thickness becomes less than the penetration depth of the exciting beam.

5. Discussion

5.1. Chemical composition

X-ray diffraction data was used to determine chemical composition in the InGaN/GaN MQW and AlGaN samples. In the InGaN/GaN MQW nanowire sample, 4 different methods were used to see inside the sample at a particular position (denoted by the red circle in Fig. 2a). While the information afforded by destructive methods such as STEM and cross-sectional EDX (Fig. 2b and c, respectively) can be extremely valuable, research samples such as these are expensive to produce and sacrifice is not always desirable, especially when the structures have-been contacted or incorporated into a monolithic device.

CL results (Fig. 2e) gave good information about the exciton behavior in the MQW structure, but to obtain the chemical composition from the CL exciton peak requires additional and often uncertain information about the specific material and MQW structure, such as confinement, strain effects, and bowing parameters. In contrast, the X-ray diffraction data in Fig. 2f, along with elastic constants determined by our growth conditions, gives complete chemical data, which was correlated by the destructive EDX measurement. X-ray diffraction was also used to ensure that the indium-rich nanowire existed throughout the length of the ridge, which would have been difficult to confirm using cross-sectional methods.

For the AlGaN sample, X-ray diffraction was used to create a complete chemical map of the ridge region (Fig. 3c). Diffraction conditions were optimized for the center nanoridge, and nanoridge locations where the signal appears to be missing denote growth where the crystallographic orientation is different enough that these diffraction conditions don't produce noticeable signal. This data was left “missing” to emphasize the orientation information (discussed below), but the diffraction conditions were later optimized for each ridge to provide complete chemical data (not shown).

5.2. Crystallographic orientation

The diffraction data on the InGaN/GaN MQW sample in Fig. 2d showed us that the lattice orientation was extremely uniform across the ridges, indicating that our growth conditions here would be excellent for coalescence by overgrowth.

The orientation data for the AlGaN sample was also informative. Fig. 3b shows that our AlGaN lattice was elastically strained on top of the GaN template, indicating an extremely high quality AlGaN/GaN interface. This makes our growth conditions promising for AlGaN/GaN nanoHEMT applications, and we managed to evaluate them without contacting or destructive methods. Fig. 3d used 3-dimentional reciprocal space mapping to compare data for three different ridges in one space. The figure clearly shows complete reciprocal space data for 3 different signals, similar in quality, but separated in crystallographic orientation. These growth conditions would not lend themselves well to coalescence.

The planar orientation data for the GaN-on-AlN sample was also very interesting, and raises certain questions about the mechanisms of growth and coalescence. The very strong 0-tilt signal indicates a presence of flat, high quality GaN, but the signals displaced in χ reveal

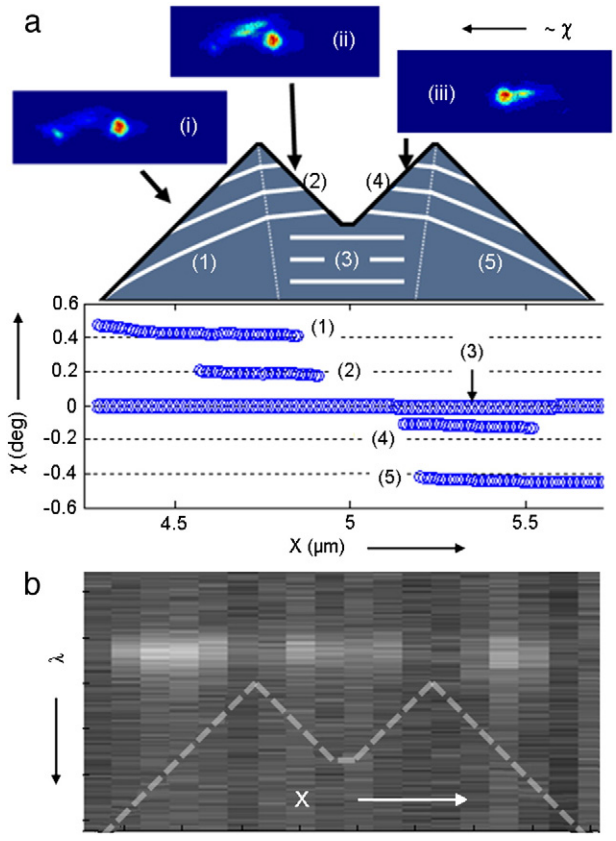

Fig. 4. a) Diffraction signal χ distribution for different positions across the 2-ridge structure in our GaN-on-AlN sample. The horizontal axis corresponds approximately to the χ angle and the vertical axis corresponds approximately to the 2θ angle. (i), (ii), and (iii) denote CCD signal images for selected locations, and the Arabic numbering (1)–(5) shows which signals arise from which planar orientations. b) 18 CL spectra, taken at different positions across the 2-ridge structure. The dotted line represents the ridge structure profile to make it easier to read.

the presence of other crystallographic orientations inside our 2-ridge structure. The overall pattern indicates that planes laterally far from the nucleation site bend slightly to relieve strain, but the bending is much less at the sites of coalescence, indicating that this effect likely arises from the final cooling phase of the growth process.

6. Conclusions

Sub-micron beam X-ray diffraction was used on a variety of nanoscale group III-nitride samples and was shown to have unique advantages in discerning chemical composition and planar orientation on the nano scale. Chemical composition could be determined directly and without interference by other effects, and planar orientation could be easily and thoroughly studied. Additionally, the small size of our beam spot made direct spatial mapping of nanostructure properties possible. All of this was done without destroying the valuable and expensive-to-produce samples.

The high intensity and small beam footprint makes this a useful technique for any situation where one would like to study the lattice of specific nanostructures, rather than having to illuminate many structures at once for want of signal or spatial precision. The technique is not without limitations, however. Immense beam intensity is required to obtain adequate signal from tiny structures, necessitating a synchrotron-based light source, which not all research groups have access to. Additionally, X-ray diffraction measurements are very sensitive to incident photon angle, and the focusing necessarily creates a “momentum spread” which will decrease our angular resolution. All things equal, a smaller beam footprint means more dramatic beam convergence, the effect being that there will always be a trade-off between angular and spatial resolution.

References

[1] D. Zubia, D. Hersee, J. Appl. Phys. 85 (1999) 6492.
[2] S. Fafard, K. Hinzer, S. Raymond, M. Dion, J. McCaffrey, Y. Feng, S. Charbonneau, Science 274 (1996) 1350.
[3] J.-Y. Marzin, J.-M. Gérard, A. Izraël, D. Barrier, Phys. Rev. Lett. 73 (1994) 716.
[4] Y. Arakawa, IEEE J. Sel. Top. Quantum Electron. 8 (2002) 823.
[5] K. Nishizuka, M. Funato, Y. Kawakami, Sg. Fujita, Y. Narukawa, T. Mukai, Appl. Phys. Lett. 85 (2004) 3122.
[6] B. Neubert, P. Bruckner, F. Habel, F. Sholz, T. Riemann, J. Christen, M. Beer, J. Zweck, Appl. Phys. Lett. 87 (2005) 182111.
[7] A.A. Sirenko, A. Kazimirov, A. Ougazzaden, S. O'Malley, D.H. Bilderback, Z.-H. Cai, B. Lai, R. Huang, V. Gupta, M. Chien, S.N.G. Chu, Appl. Phys. Lett. 88 (2006) 081111.
[8] P.L. Bonanno, S.M. O'Malley, A.A. Sirenko, A. Kazimirov, Z.-H. Cai, T. Wunderer, P. Brückner, F. Scholz, Appl. Phys. Lett. 92 (2008) 123106.
[9] M. Hanke, M. Dubslaff, M. Schmidbauer, T. Boeck, S. Schöder, M. Burghammer, C. Riekel, J. Patommel, C.G. Schroer, Appl. Phys. Lett. 92 (2008) 193109.
[10] A. Kazimirov, A.A. Sirenko, D.H. Bilderback, Z.-H. Cai, B. Lai, R. Huang, A. Ougazzaden, J. Phys. D: Appl. Phys. 39 (2006) 1422.
[11] P.L. Bonanno, S. Gautier, A.A. Sirenko, A. Kazimirov, Z.-H. Cai, W.H. Goh, J. Martin, A. Martinez, T. Moudakir, N. Maloufi, M.B. Assouar, A. Ramdane, L. Le Gratiet, A. Ougazzaden, Nucl. Instrum. Methods Phys. Res., Sect. B 268 (2010) 320.
[12] S. Gautier, C. Sartel, S. Ould-Saad, J. Martin, A. Sirenko, A. Ougazzaden, J. Cryst. Growth 298 (2007) 428.
[13] M. Schuster, P.O. Gervais, B. Jobst, W. Hösler, R. Averbeck, H. Riechert, A. Iberlk, R. Stömmerk, J. Phys. D: Appl. Phys. 32 (1999) A56.
[14] S.P. Łepkowski, J.A. Majewski, G. Jurczak, Phys. Rev. B: Condens. Matter Mater. Phys. 72 (2005) 245201.